Environ Res Tec, Vol. 7, Issue. 4, pp. 547–563, December 2024

Environmental Research and Technology
https://ert.yildiz.edu.tr - https://dergipark.org.tr/tr/pub/ert
DOI: https://10.35208/ert.1472406

Environmental Research & Technology

Research Article

Study on defluoridation of water by using activated carbon derived from chestnut shell as adsorbent

Firdous Ahmad DAR, Kurella SWAMY*

Department of Chemical Engineering, National Institute of Technology Srinagar, Jammu and Kashmir, India

ARTICLE INFO

Article history
Received: 23 April 2024
Revised: 06 May 2024
Accepted: 16 May 2024

Key words:
Activated carbon; Adsorption; Characterization; Fluoride; Water remediation

ABSTRACT

The present work intended to produce new cost-effective alkali-activated adsorbents from chestnut shells with the purpose of removing fluoride from water, and to explore the effect of pyrolysis temperature on fluoride decontamination at different operational and environmental parameters. The microstructure and morphological characteristics of the resulting activated carbons were thoroughly investigated using BET, FTIR, XRD and SEM. The effectiveness of the prepared adsorbent materials in treating and remediating fluorinated water was evaluated. The impacts of several factors, including the dose of the adsorbent, the initial contamination level of fluoride, and pH on the fluoride removal efficiency were investigated. In accordance with the data, the highest adsorption was found to be at a 6 pH during 5 hours of processing duration and 0.5 g/L of dosage of adsorbent. The experimental results were well-fit by the Freundlich isotherm model and the pseudo-second-order kinetic model. The highest fluoride removal efficiency was found to be 78% at adsorption medium pH 6 and initial fluoride concentration of 10 mg/L by the adsorbent prepared at 800°C. Additional research on adsorption along with rejuvenation revealed that the reduction in adsorption potential to 10% following four repetitions of operation involving regeneration, thereby showcasing the adsorbent's versatile applicability for repeated use.

Cite this article as: Dar FA, Swamy K. Study on defluoridation of water by using activated carbon derived from chestnut shell as adsorbent. Environ Res Tec 2024;7(4)547–563.

INTRODUCTION

The occurrence of fluoride within water supplies is currently identified as one among the most serious worldwide water-related concerns, making the development of efficient technology for eliminating it a crucial concern for enhancing the well-being of humans in afflicted regions. Adsorption has risen to prominence as a popular method for removing fluoride from water, and it has garnered a lot of interest in recent years due to the fact that it is an effective, economical remediation method along with its easiness to apply. Although fluoride can help people to strengthen the ortho skeletal and dental structures when consumed in appropriate amounts, too much consumption of it can have serious negative effects on the well-being of people [1, 2]. Particularly, ample proportions of fluoride have associated with a variety of medical challenges, including tooth and bone fluorosis, malignancy, osteoporosis, arthropathy, cerebral and mental disorders and other neurological ailments [1, 3–6]. The poisoning of waterways with fluoride influences a great number of nations all over the world; nevertheless, the most serious issues have been identified in Tanzania, Bangladesh, Pakistan, India and Ghana [7–9]. In all, around 200 million individuals in 28 nations have been adversely impacted, this issue being especially severe in some of those nations [10, 11]. In Tanzania, 30% of the drinkable water had fluoride concentration more

***Corresponding author.**
*E-mail address: kurellaswamy@nitsri.ac.in

than 1.5 mg/L [12, 13]. There should be no more than 1.5 mg of fluoride per litre in water used for drinking, according to guidelines established by the World Health Organization including the European Commission (EC Directive 98/83/EC) [14]. In India, the concentration of fluoride in water is contingent upon geological factors and ranges from 0.5 to 48 mg/L as the naturally existing fluoride content in water, varying due to different geological parameters. In India, 19 states exhibit high fluoride levels in groundwater, surpassing 40 mg/L. In Churu (RJ) the fluoride level in ground water is determined to be 30 mg/L, while in Nagaur (RJ) it is round 44 mg/L. The states with F^- levels surpasses the WHO guidelines include Uttar Pradesh, Gujarat, Rajasthan, Madhya Pradesh, Haryana, West Bengal, Andhra Pradesh, Telangana, Maharashtra, Punjab, Karnataka, Tamil Nadu, and others [4]. It is believed that the efficient elimination of fluoridated water is a challenging and inspiring topic, particularly in the above locations.

Many fluoride removing strategies, including membrane separation [15, 16], ion-exchange [17], coagulation [18], precipitation [19, 20] and adsorption [21] are currently implemented and used. Despite their usefulness, several of these techniques have limitations. In particular, ion exchange isn't the most successful or cost-efficient approach because of the expense of the resin and relatively limited selectivity, along with the fact that it has to be constantly regenerated [22]. The usage of membranes comes with its own set of problems such as the expensive nature of the membranes themselves, high expense of cleaning and controlling fouling [4, 23]. This makes the procedure rather costly to operate [24, 25]. Alternately, coagulation has its drawbacks despite being a cheap method since it requires large dosages, which leaves behind significant leftover quantities of aluminium [22]. On the contrary, it has been claimed that the precipitation technique may be used towards the fluoride removal. This approach is particularly effective when calcium, aluminium, or ferrous salts are used; however, the poor solubility of these produced compounds restricts the potential for fluoride removal [22, 26]. Because of the above reasons, adsorption has been proved to be the best way to get elimination of fluoride because it has several benefits compared to alternatives [26–28]. In particular adsorption is the best approach as it is inexpensive, easy to use, more selective, and readiness of adsorbent.

There are many different types of adsorbents that have been utilized [15, 23, 26, 29]. These include expensive materials like ion exchange resins [30], activated carbon (AC) [31–33], more affordable ones like carbon nanotube fibers [34, 35], bone charcoal [36], fly ash [37] and clay [38] etc. Among such options, activated carbon appears to be proven most useful due to its most of the beneficial properties. These include a wide specific area for adsorption, great porosity and elevated catalytic efficiency [39, 40]. Activated carbon does have certain benefits, but it is not very effective at removing inorganic contaminants like fluoride due to its limited sorption capability and lack of selective ability. In recent times, a significant number of authors have included in their work about the transformation of activated carbon materials using a variety of chemicals with an effort to circumvent this constraint.

In order to improve activated carbon's efficiency towards the defluoridation, it has lately been processed using silicates [41, 42], magnesium oxide [43], lanthanum oxide [44, 45] and aluminium oxide [46]. In aforementioned substances, lanthanum shows the greatest promise; however, lanthanum oxide is quite pricey, consequently it might be more practical to combine lanthanum oxide using less pricey metallic substances (such as magnesium, silicon, calcium, etc.) on activated carbon for generating mixed metal based modified activated adsorbents having a significant ability for adsorption [47]. However, magnesium modified adsorbents are recommended since they are cheap and show excellent adsorption ability towards defluoridation throughout a broad range of pH (i.e. 2–10) [18, 48]. For the elimination of arsenate and fluoride, magnesium (Mg) has been shown to combine using lanthanum on hydrotalcite in earlier researches [49]. However, such compounds are no longer used because of the high price of unadulterated magnesium salts used primary reagents [50]. Despite magnesium oxide has lower cost and impressive fluoride adsorption capabilities [51], its fine particle size enhance the surface area and could boost the fluoride removal ability [52]. Due to this, adding magnesium to modify the activated carbon could boost overall stability besides maximizing overall advantages of it.

Based on the aforementioned information, chestnut shell adsorbent (CSAC) was developed. The material's efficacy towards defluoridation was tested in batch studies. Within the context of this research, it has been investigated the defluoridation capacities of activated carbon produced from chestnut shells. This study involved an exploration of the influence of many factors, including water pH, initial content of fluoride and adsorbent dosage. Whereas scanning electron microscopy (SEM), Fourier transform infrared spectroscopy (FTIR) and X-ray diffraction (XRD) were used to examine the morphological and structural characteristics of the activated carbon. The adsorption mechanism was also described using kinetic and isotherm models.

MATERIALS AND METHODS

Materials

Analytical-grade reagents were utilized throughout the experimentation. The fluoridated water mixture was prepared by using anhydrous sodium fluoride (NaF) supplied by Merck. A standard sample solution calibrated to a proportion of 1000 mg/L had been obtained by mixing 2.210 grams of sodium fluoride with 1000 ml of distilled water. Then the original solution was diluted in order to produce the solutions having appropriate level of fluoride content.

Preparation of Activated Carbon

The research found that activated carbon synthesized from chestnut shells required impregnations to be effective and it was done following by the procedures reported in the litera-

ture [18]. The chestnut shells were cleaned by distilled water for the elimination of adhering debris and other unwanted materials attached to them before being dried overnight approximately at 100°C to minimize moistness percentage [53]. The dehydrated product was crushed and screened until its particulate diameter was uniformly about 0.45–0.15 mm. The chestnut shell material that was prepared was designated as CS. Then it was kept at ambient temperature for 24 hours, 20 g of dried chestnut shells was soaked using 250 ml of the potassium hydroxide (2 M), which was used as the activating agent. After filtering, the material had been placed into furnace. The activation of the precursor was done by using pyrolyzer; carbonization was undertaken at 600°C, 700°C and 800°C and was maintained for 2 hours during entire process, with a consistent heating flow of 99% purity of nitrogen gas supply. Following, cooled carbonized residues have been cleaned using milli-Q distilled water until neutral pH, while the pH 7 was maintained consistent (using HP pH meter, model CRISON 602) [53, 54]. The resulting activated material, after carbonization, was subsequently heated in an oven for drying at a temperature of 100°C for 24 hours so as to get the final activated carbon products (CSAC600, CSAC700 and CSAC800).

Analytical Determinations/ Quantitative Findings

The SPADNS spectroscopic approach [50] was used to determine the fluoride residual content. This technique involves the interaction among F^- ions with Zirconium, which separates a portion of F^- ion form a colorless (ZrF_6^{2-}) anionic compound as well as colored agent. When comparing with conventional fluoridated sample, the color generated gets gradually lighter on increasing the quantity of fluoride. The Zirconium-SPADNS complex combined compound was employed because of its high stability when exposed to the dark and its ease of preparation by combining two distinct chemicals/reagents [50]:

- Reagent 1 was prepared by combining 958 mg of SPADNS (2-(4-Sulfophenylazo)-1, 8-dihydroxy-3, 6-naphthalene disulfonic acid trisodium salt) with 500 ml of distilled water. The SPANDS was supplied by Sigma Aldrich.
- Reagent 2 was prepared by mixing 133 mg of Zirconyl chloride hydrate with 25 ml of distilled water. Then the 350 ml of hydrochloric acid (HCl) was added to the above and additional distilled water was also added to make a total volume of 500 ml solution. The Zirconyl chloride hydrate was supplied by Sigma Aldrich and HCl was supplied by CDH.
- Reagent 3 (Zr-SPADNS), a complex mixture, was prepared by combining equal volumes of reagent 1 and reagent 2. The mixture was stored in a dark environment as it can remain stable for approximately 2 years in the dark environment.

After that, 2 ml of Zr-SPADNS solution was poured into ten milliliters of deionized water, which serves as blank, and subsequently into ten milliliters of specimens that have been diluted with water. The mixture has been thoroughly combined after each addition.

Characterization Approaches

Activated carbon material had been examined regarding their surfaces morphological structures utilizing Scanning Electron Microscope (Jeol JSM-6390 LV) alongside energy dispersive X-ray system (EDS). Following standard experimental conditions, the crystallographic structure was determined by X-ray diffraction (XRD) (Bruker D8 FOCUS). For the study of the chemistry of bonds on chestnut shell was analyzed by Fourier Transform Infrared Spectroscopy (FT-IR) (Perkin Elmer). At a temperature of 77 K, the Brunauer, Emmett, and Teller (BET) analytical program was utilized to figure out the specific surface area. The adsorbent was analyzed both proximally and ultimately. The proximate analysis comprised the percentage of moisture, volatile matter, carbon content matter and leftover non combustible residue in the form of ash. The ultimate Analysis of elements in biochar samples was performed using CHNSO Elemental Analyzer.

Adsorption Studies

Fluoridated samples in beakers have been subjected to adsorption studies with varying proportions of adsorbent added under steady temperature. The substance was stirred using magnetic stirrer at a steady rate of 80 revolutions per minute (rpm). Throughout the course of the examinations, a variety of experimentation process parameters, including pH (ranging from 3 to 9), commencing concentration of fluoride (ranging from 2 to 10 mg/L), adsorbent dosage (ranging from 0.1 to 1.0 g/L) and contact duration (24 hours for kinetics and equilibrium), were individually and separately altered as the ranges of parameters were chosen based on the literature [27, 55]. Adsorbate was removed from examined specimens of water by passing them through filter papers with a pore diameter of 45 μm, whereas the fluoride leftover level was one of many characteristics measured within the resulting filtrate. The average of 3 replicated and separate investigations are resulted in these findings. Eq. (1) was used to figure out the proportion of fluoride that was removed (%R).

$$\text{Removal (\%)} = \left(\frac{C_0 - C_f}{C_0}\right) \times 100 \quad (1)$$

Where C_0 represents the fluoride level of pre treated water sample (mg/L), and C_f represents the fluoride content after adsorption (mg/L).

Below Eq. (2), was used to figure out the adsorption capability Q_e (mg/g) of the sorbent.

$$Q_e = \left(\frac{C_0 - C_e}{m}\right) \times V \quad (2)$$

Where C_e (mg/L) represents the level of fluoride after treatment, V (L) corresponds to the volume of the untreated sample, while m (g) depicts the adsorbent dosage mass that is being utilized.

Equilibrium Experiments

All isothermal tests were conducted by adding a constant dosage of adsorbent (g) to 200 mL contaminated sample with fluoride level (2–10 mg/L) in 250 ml beakers. The findings of the experiments were analyzed by using the Langmuir, Freundlich and Temkin isotherm models respectively to account for

the data on adsorption. The equation for the Langmuir model is represented by Eq. (3). The Langmuir model establishes a correlation between the fluoride level of the liquid after the equilibrium and the uptakes of the solid phase adsorbate (Qe).

$$Q_e = \frac{Q_m K_L C_e}{1+K_L C_e} \quad (3)$$

Where Q_m (mg/g) is the theoretically calculated monolayer/maximal adsorption rate, while K_L (L/mg) corresponds to the energy of fluoride sorption.

According to the model developed by Langmuir, the adsorbent is assumed to have a finite adsorption potential (Q_m) and the adsorbate develops a monolayer over the exterior of the adsorbent, while no or little interactions exists among the deposited contaminants.

The Freundlich model relates equilibrium amounts of fluoride (mg/L) to adsorption capabilities of Q_e (mg/g) of adsorbent which may be stated as Eq. (4):

$$Q_e = K_f C_e^{\frac{1}{n}} \quad (4)$$

Where K_f is a constant associated with adsorption efficiency and 1/n represents another constant parameter associated with the amount of adsorption intensity that takes place or the heterogeneousness of surface, values of 1/n >1 suggest cooperative adsorption, whereas 1/n=0 denotes a heterogeneous phase and 1/n <1 then the Freundlich isotherm is normal.

The Temkin isotherm equation corresponds to a three factor model represented as Eq. (5) that has been employed to match the observational data.

$$Q_e = \frac{RT}{B_t} \ln (a_t C_e) \quad (5)$$

Where Q_e (mg/g) represents the equilibrium adsorbed quantity, C_e (mg/L) is the adsorbate equilibrium quantity, and a_t denotes the variability coefficient, which ranges from 0 to 1. This formula is applicable across a wide range of concentrations in a solution; while it fails to comply with Henry's rule for low levels because it adequately changes to a Freundlich isotherm, it does anticipate a monolayer adsorbance of the Langmuir isotherm for elevated concentrations.

Kinetics Studies

The pseudo-first-order (PFO) and pseudo-second-order (PSO) kinetics for adsorption of ions of fluoride have been explored, and appropriate resulting adsorption kinetic parameters were then subsequently evaluated to quantify the sorption rates and further found the appropriate expression rates indicative of potential interaction mechanisms. The pseudo-first-order and pseudo-second-order approaches utilized during the data assessment have been depicted in Eq. (6) and Eq. (7):

$$Q_t = Q_e\left(1- e^{-k1t}\right) \quad (6)$$

$$Q_t = \frac{k_2 Q_e^2 t}{1+k_2 Q_e t} \quad (7)$$

Where, the adsorbed quantity of fluoride after equilibrium time t (minutes) is denoted by Q_t and Q_e (mg/g). The pseudo-first-order rate constant, k_1 is denoted in units as L/min; the pseudo-second-order rate constant, k_2 is written in units as g/mg/min; while t, in minutes represents the overall interaction duration.

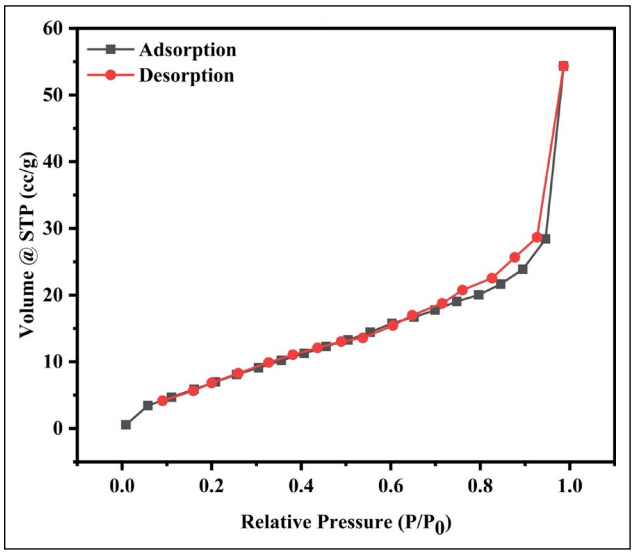

Figure 1. Nitrogen adsorption-desorption isotherms of CSAC800.

RESULTS AND DISCUSSION

Analysis of Activated Carbon

BET Analysis

The experimental outcomes revealed that the CS surface exhibited mesoporous surface appearance, featuring multiple pores and an irregular, block-shaped configuration. In comparison, CSC800 exhibited a surface that was noticeably rough and contained a large number of pores. The presence of these pores was a direct result of the volatiles emission during pyrolysis. The CSAC800 surface displayed a broken and irregular texture, characterized by the presence of multiple well-defined pore structures. The interaction between KOH and the biomass led to a significant reduction in the pore size of CSAC800. This interaction stimulated the production of small molecular gaseous substances (H_2, CO and CO_2). Cations of alkali metals produced have the ability to insert themselves into the partially formed char material, which enhances the breakdown and fragmentation of the biochar [56]. The findings clearly elucidate that the transformative impact of pyrolysis pretreatment with KOH wielded a profound influence on the captivating morphology of biochar, resulted in notable alterations in its morphology.

The adsorption isotherms of three specific variants CSAC600, CSAC700, and CSAC800 displayed Type IV isotherm as represented in Figure 1 providing confirmation of the presence of macropores [57] and in conjunction exhibiting an h4 hysteresis indicating mesoporous arrangements or configurations that were created upon the outermost layer of biochar derived from chestnut shells that were activated using KOH [58]. The range of pore diameters found in CSAC600, CSAC700, and CSAC800 spanned ranging between 2 to 50 nm, thereby ensuring the adsorbent's mesoporous characteristics. The measured values for CSAC800 included a specific surface area (SSA) of 912.38 m^2/g, pore volume of 0.188 cm^3/g and pore diameter of 11.131 nm as detailed in Table 1. Compared to CS, notable enhancements

Table 1. The specific surface area (SSA), pore volume, and diameter of various adsorbents were determined, utilizing parallel experimental investigations to ensure accuracy and reliability and the data are presented as the average of two specimens along with the corresponding standard deviation

Adsorbent	SSA (m^2/g)	Pore volume (cm^3/g)	Pore size (nm)
CS	3.76	0.0318	0.0293
CSC800	15.12	0.056	3.637
CSAC600	472.58	0.096	8.342
CSAC700	785.80	0.149	9.021
CSAC800	912.38	0.188	11.131
CSAC800-F^-	680.16	0.112	8.751

in specific surface areas (SSA) were observed in CSC800, CSAC600, CSAC700, and CSAC800. CSC800 exhibited a 4.02 times increase, while CSAC600, CSAC700, and CSAC800 displayed remarkable improvements of 125.68, 208.99, and 242.65 times in their respective specific surface areas. Similarly, the pore volumes of CSC800, CSAC600, CSAC700, and CSAC800 exhibited significant increments of 1.76, 3.09, 4.80, and 6.06 times respectively. The BET analysis yielded compelling evidence that the alkali-activated biochar derived from chestnut shells showcased remarkable enhancements in specific surface area and the presence of mesoporous structures. Consequently, the material exhibited a plethora of highly effective interfacial adsorption sites, offering ample opportunities for the efficient adsorption of target compound (fluoride).

FT-IR/ Functional Group Study

The FTIR spectra of CS revealed distinctive spectral features as depicted in Figure 2. The peak observed at 1460 cm^{-1} was associated with the deformation vibration of -CH_2 groups. Moreover, distinctive spectral peaks were discerned at 1083 cm^{-1}, 1244 cm^{-1}, 1640 cm^{-1}, 2927 cm^{-1}, and 3423 cm^{-1}, aligning with the stretching vibrations of C-O-C, C-O, C = O, C-H, and -OH groups, respectively. These observations furnish valuable knowledge about the molecular composition and structural characteristics of CS [58–60]. Nonetheless, the FTIR peak intensities observed in CSC800 and CSAC800 were markedly diminished as a consequence of the utilization of a high pyrolytic temperature. This finding aligns consistently with the outcomes of a prior investigation, reinforcing the correlation between elevated pyrolytic temperatures and reduced FTIR peak intensities [61]. As the temperature at which calcination occurs increased, the patterns observed in the spectrum parameters of the adsorbents showed stronger magnitudes for the peaks located at 1083 cm^{-1} and 1630 cm^{-1}. This phenomenon can be attributed to the activation of alkali compounds.

Importantly, the distinct spectra in the Fourier-transform infrared (FTIR) spectroscopy at 1421 cm^{-1}, which corresponds to the stretching vibration of C = C bonds, was solely detected in CSAC800. Importantly, the distinct peak

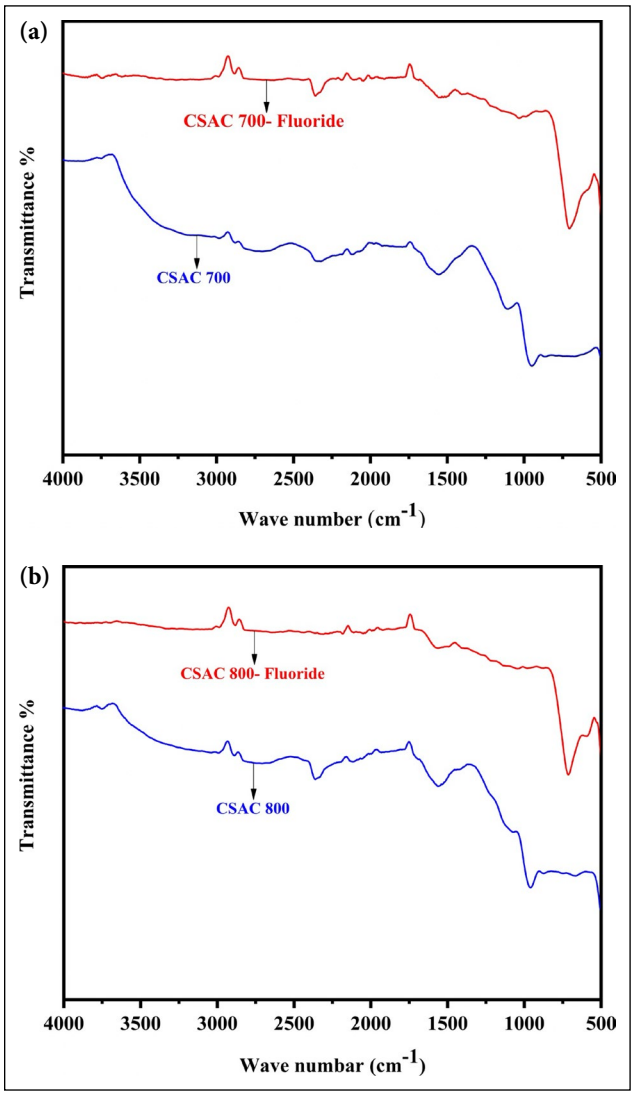

Figure 2. **(a)** FTIR spectra of activated carbons CSAC700 derived from chestnut shells. **(b)** FTIR spectra of activated carbons CSAC800 derived from chestnut shells.

in the Fourier-transform infrared (FTIR) spectroscopy at 1421 cm^{-1}, which corresponds to the stretching vibration of C = C, was solely noticeable in CSAC800. After adsorption the peak at 993 cm^{-1} shifted to 710 cm^{-1}.

Scanning Electron Microscopy (SEM)

Scanning Electron Microscopy (SEM) was employed to analyze and track the surface characteristics, texture and the micro-structural features and changes occurring in the materials. The surface-morphology of AC, which were obtained from chestnut shells are shown in Figure 3 since the aforementioned substances were shown to comprise the most effective material for adsorption throughout the studies that followed. The chestnut shell carbons exhibited a uniform and well-defined structure characterized by a prevalence of macropores, showcasing an average pore diameter of 12 µm [62]. In accordance to an investigation examining the morphology of activated carbon, it appears that the C-KOH bonding generates an extensive density of microscopic

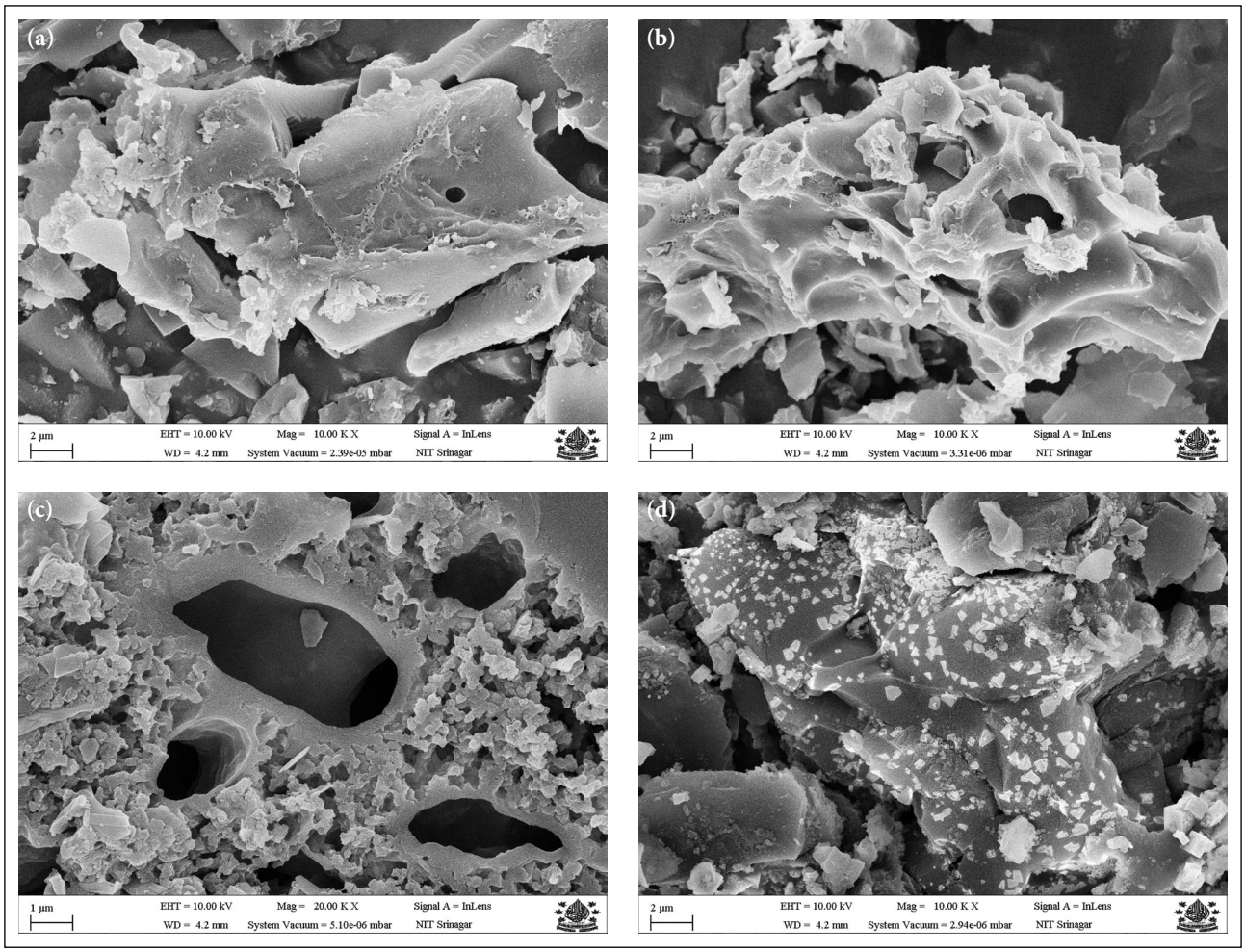

Figure 3. **(a)** SEM images of chestnut shell activated carbon CSAC700 before adsorption. **(b)** SEM images of chestnut shell activated carbon CSAC700 after adsorption. **(c)** SEM images of chestnut shell activated carbon CSAC800 before adsorption. **(d)** SEM images of chestnut shell activated carbon CSAC800 after adsorption.

pores, which substantially boosts the overall surface vicinity and capacity among those pores [63]. Additionally, the pore spaces within activated carbon exhibit irregular configurations that might serve as adhering surfaces for adsorption agents of varying dimensions. The adsorbent produced during the present investigation might come in a range of forms, including those with varying porosity, wall dimensions and patterns as shown in Figure 3. The activation procedure resulted in considerable removal of organic matter and subsequent porosity formation. Figure 3 also displays the SEM images comprising the CSAC700, and CSAC800.

The visualizations reveal cavernous cavities running across every specimen, which is suggestive regarding spontaneous activation-induced gasification for volatile materials. These AC specimens had been entirely composed by accumulated high-quality particulates, implying that it might be crucial for adsorption towards fluoride ions within various contaminated solutions. As was already mentioned, the disintegration of carbonates formed while the calcining operation is what is responsible for those morphological alterations. From Figure 3b, one can easily observe a uniform dispersion of fluoride adsorption throughout its entire area following fluoride adsorption. Additionally, respective SEM representations appeared after fluoride adsorption across the exteriors of competing adsorbent elements, in addition to the above it is clear that the CSAC's interface has adsorbed a higher proportion of fluoride from solution.

XRD Analysis

The X-ray diffraction (XRD) peaks detected at 2θ = 14°, 20° and 39° can be correlated to the presence of the non-crystalline carbon (002) structure and graphitic carbon lattice planes (100) respectively according to Figure 4. Distinctive prominent XRD peaks corresponding to the crystallographic appearance of cellulose in CSAC were identified at angles of 16.06°, 21.82°, and 34.56°, which revealed that cellulose, had completely decomposed [64]. The disappearance of a distinct dispersion pattern at 30.16° indicates that there are no metallic inclusions embedded over the activated carbon's surface. Additionally, the relatively low intensity of the peak in activated carbon pointed to the fact that majority of the chestnut shell underwent decomposition to a state of carbon lacking crystalline structure throughout the process of alkali-activated pyrolysis. The existence of a carbon structure characterized by amorphous or disordered properties promoted the availability of additional adsorption sites to enhanced adsorption capacity.

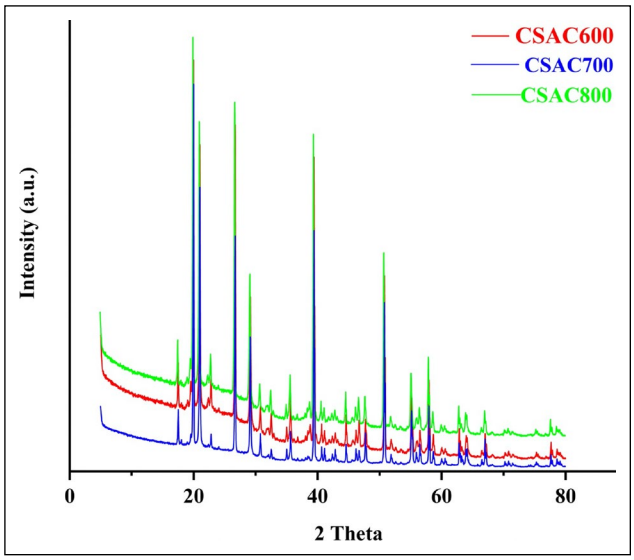

Figure 4. XRD profiles of activated carbons derived from chestnut shell.

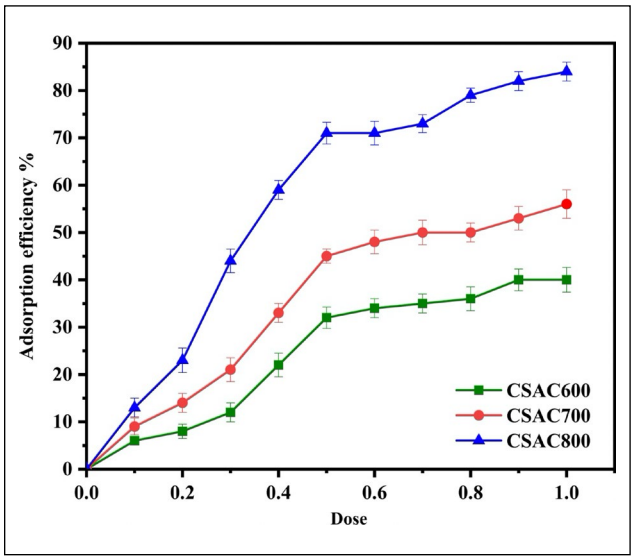

Figure 5. Effect of adsorbent dose on F^- adsorption (Ci 10 mg/L, pH 7.0±0.1, time= 24 h, T= 25±1 °C).

Batch Adsorption Experiment

Effect of the Dosage/ Impact of Adsorbent Dosage Along with Adsorbent Comparison

Following the qualitative detection of fluoride adsorption on chestnut activated carbon, various quantitative examinations were conducted. In a series of batch experiments, the impact of varying dosage of activated carbon adsorbent was investigated and studied to understand how the adsorbent's quantity influences its capability to mitigate the fluoride contamination in the solution and to assess its potential for removing fluoride ions (F^-) effectively. The optimal adsorbent quantity was obtained by altering the adsorbent dosage falling between 0.1 to 1.0 g/L, while maintaining the constancy of all other factors. The efficacy of the removal, in relation to both the remaining fluoride concentration and associated percentages, is graphically represented in Figure 5. To evaluate the influence of varying adsorbent levels, 25 ml of adsorbate mixture containing 10 mg/L had been taken around 7 pH. The resulting mixture was then equilibrated using 0.1 to 1.0 g of CSAC over 24 hours.

From Figure 5, it is evident that as the quantity of sorbent employed went up from 0.1 to 1.0 g/L; there was a corresponding increase in the adsorption capacity. Because there were more active spots available, it became apparent that fluoride adsorption enhanced when CSAC dosage rose. Alterations within elimination process could possibly be attributed to the initial contaminant level, during which each adsorbent spot remained unoccupied. As illustrated, upon elevating the adsorbent quantity, the elimination percentage of fluoride surged to 78% at a 6 pH for the CSAC800 adsorbent. This led to a left-behind level of fluoride falling to 2.2 mg/L, accomplished by employing under 0.5 g/L of the specified adsorbent. For the correlation, an adsorbent named CSC800 was meticulously formulated and the adsorption efficiency by CSC800 was around 20%. This showed that the activation agent had a greater impact on

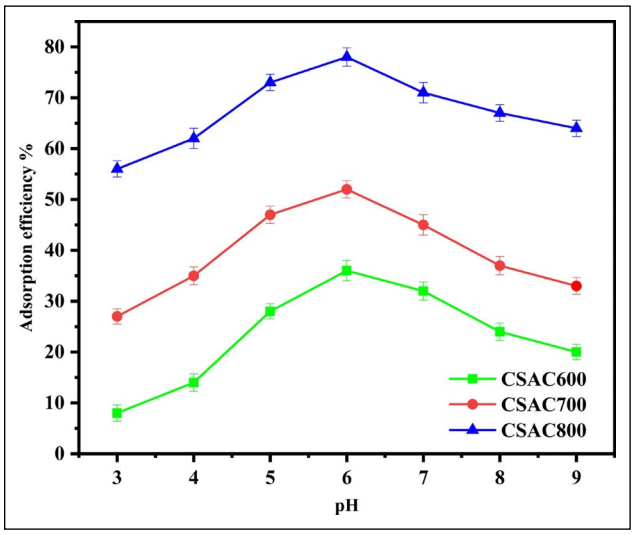

Figure 6. Effect of pH on F^- adsorption (Ci 10 mg/L, dosage 0.5 g/L, time 24 h, T=25±1 °C).

the adsorption process. Yet, when the quantity of sorbent used exceeds beyond 0.5 g/L, the active sites of adsorbent reached their limit, resulting in a substantial decrease in the fluoride concentration left in the solution, which in turn weakened the effectiveness of the adsorption process. To account for both the amount used and the remaining concentration, a dosage of 0.5 g/L for CSAC800 was chosen for subsequent experiments.

Effect of the Initial pH

The pH level of solution had a notable influence on the characteristics of the adsorbent's surface. The impact of pH on the adsorption of fluoride onto chestnut activated carbons was examined by altering the solution's pH within the range of 3 to 9. These tests were conducted with exposure time of 24 hours, at 25°C, and a dosage of 0.5 g/L. The findings from these experiments are presented

Table 2. Evaluating the adsorptive capabilities of CSAC800 comparative to several adsorbents documented in published works for defluoridation

Adsorbent	Initial concentration mg/L	Adsorbent dose	pH	Temp. °C	Equilibrium time (min.)	Surface area m^2/g	Applicable isotherm models	Adsorption capacity/ efficiency	Ref.
γ-Al_2O_3 hollow tubular alumina	100	50 mg/L	3	30	1440 min.	306.14 m^2/g	Freundlich	84.25 mg/g 75%	[69]
Sawdust impregnated ferric hydroxide and activated alumina	5–50	0.1 g/10ml	6.5	30	240 min.	22.5 m^2/g	Freundlich	2.42 mg/g 74%	[70]
Activated alumina	5 mg/L	0.4 g/L	6–8	25	1440 min.	198 m^2/g	_	35 mg/g 69%	[71]
Hydroxyl aluminum oxalate (HAO)	10 mg/L	1 g/L	6.5	24	239 min.	68.34 m^2/g	Langmuir	400 mg/g 75.9%	[72]
Zirconium phosphate	1–10	2 g/L	2–12	30	60 min.	129 m^2/g	Langmuir	4.268 mg/g 76%	[73]
Lanthanum-modified pomelo peel biochar	10 mg/L	1.0 g/L	5.2	25	1440 min.	506.30 m^2/g	Freundlich	7.62 mg/g 82%	[74]
Crushed oyster shells modified AC	10 mg/L	20 g/L	7±0.1	30	1440 min.	_	Freundlich	1.5 mg/g 76%	[75]
Mytilus coruscus shells	50 mg/L	3.33 g/L	5	25	360 min.	4.363 m^2/g	Langmuir	82.93 mg/g 56.9%	[76]
Magnesium modified coconut shell	10 mg/L	0.2 g/L	8	25	240	680.16 m^2/g	Langmuir-Freundlich	36.56 mg/g 16%	[50]
Activated carbon derived from chestnut shell	10	0.5	6	25	300	912.38 m^2/g	Freundlich	60.058 mg/g 78%	This study

in Figure 6. Within the pH range under examination, the adsorbent's ability to adsorb fluoride decreased with raising the solution's pH. Specifically, the increased adsorption capacity in acidic conditions can likely be associated with the existence of protonated hydroxyl groups. These groups have the potential to capture fluoride through a robust electrostatic attraction, leading to the formation of HF (hydrofluoric acid). At lower pH levels, the oxygen atoms present on the CSAC800 surface became protonated, leading to the formation of hydroxyl groups. Elevated amounts of hydronium ions under reduced pH likely undergo protonation in the CSAC's fundamental operation, allowing them to effectively adhere F^- ions. The interaction between hydroxyl groups and fluoride through ion exchange results in a significant uptake of fluoride [45, 65–67]. Such protonated functions are capable of attracting moisturized fluoride ions. Additional H_3O^+ F^- ion pairings may permeate the adsorbent pore surface, and F^- may also get swapped for protonated functions across the gaps. Conversely, because of fluorine's robust electronegativity, it can potentially be held in place through hydrogen bonding on the CSAC800 surface. However, this impact weakened when the pH level rose. As the pH level kept going up, CSAC800's capability to grab onto fluoride decreased quickly. As a result, a substantial percentage of the hydroxyl radicals within the solution engaged in a competitive interaction with fluoride during adsorption process. The results indicated that as the pH increased, the adsorption efficiency declined from 78% to 64% at pH range of 6 to 9. Less protonated surface spots might be accessible therefore fluoride wouldn't have been effectively eliminated when pH rose. So, it has been proposed that less adsorbate is removed throughout elevated pH environments because the anionic surface character of CSAC attracts F^- ions by electrostatically.

The literature-reported effectiveness of several adsorbents for fluoride decontamination is compared and presented in Table 2. Furthermore, CSAC800 adsorption capability was superior to other adsorbents mentioned in existing research. Yet, reaching a conclusive judgment on the effectiveness of the adsorbents proves challenging since the uptake efficiencies have been reported at various parameters. Comparing the economic viability of the material with biochars reported in the literature is additionally challenging due to variations in removal capabilities, characteristics, uses, and processing environments. Regarding softer materials, the most effective combinations were lower temperatures along with lengthy contact durations. Biochar is effectively recovered under lower temperatures as well as reduced heating cycles [27].

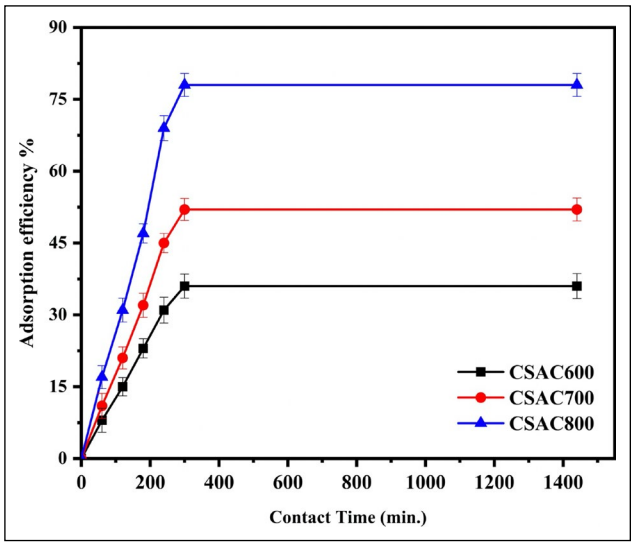

Figure 7. Effect of sorption time on F^- adsorption (Ci 10 mg/L, dosage 0.5 g/L, pH 6.0±0.1, T=25±1 °C).

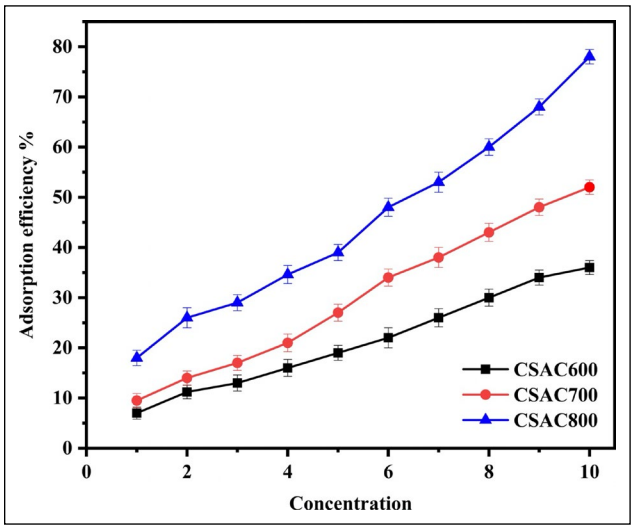

Figure 8. Effect of Ci on F^- adsorption; (Time=5 h, dosage 0.5 g/L, pH 6.0±0.1, T=25±1 °C).

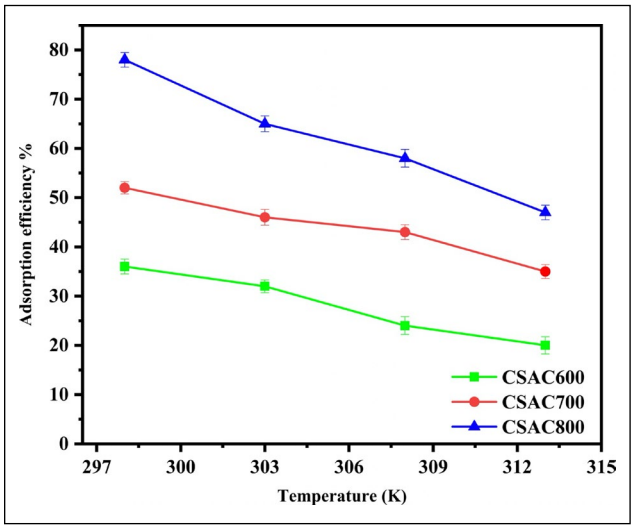

Figure 9. Effect of temperature on F^- adsorption (Ci 10 mg/L, dosage 0.5 g/L, pH 6.0±0.1, time=24 h).

Effect of Sorption Time

Another significant aspect of adsorption is how quickly the adsorbents work, so the kinetic behavior of the adsorbents represents additional important aspect for the removal mechanism; therefore, the influence of contact time has been studied and ranging from 60 to 1440 minutes (24 hours). The prolongation of the duration of the study resulted in an upward trend in the amount of fluoride that could be removed before reaching a state of equilibrium. CSAC was able to reach the steady state of sorption after 5 hours (300 minutes), and the highest fluoride adsorption effectiveness of 78% was achieved for CSAC800. The findings shown in Figure 7 revealed that once 5 hours (300 minutes) of contact time passed, there was hardly any additional improvement in fluoride removal. The fact that there exist few spots for sorption over optimum period might explain underlying cause for such phenomenon. Hence, 5 hours was chosen as the best optimal exposure period for subsequent batch experiments with chestnut shell activated carbon adsorbent materials. Importantly, this 5 hours duration proved optimal across all tested pH values.

Effect of Fluoride Concentration

Studies were conducted to determine how the adsorption was influenced by the commencing level of fluoride (2 to 10 mg/L). In this study of adsorption, overall findings that are depicted in Figure 8 pertain towards the changes that occurred in the amount of sodium fluoride that was being used. Results revealed that the degree of adsorption of fluoride varied with the level of fluoride first introduced. The study examined the impact of commencing level of fluoride (2–10 mg/L) on CSAC adsorbent (0.5 g/L) under pH 6, room temperature, along with contact period of 5 hours (Fig. 8). It was noticed that the efficiency of F^- adsorption is notably affected by the commencing level (C_i) of F^-, as shown in Figure 8. The impact of Ci was evaluated using different F^- concentrations ranging from 2 to 10 mg/L, while maintaining the other parameters like adsorbent dosage of 0.5 g/L, the exposure duration of 5 hours (300 minutes) and the pH of the solution was 6. The percentage of elimination increases as the initial F^- concentration rises. The maximal defluoridation efficacy was achieved for the adsorbent prepared at 800°C that is CSAC800. The maximal contamination elimination efficiency resulted by this adsorbent was 78%.

Effect of Temperature

The sensitivity of the adsorption process is undeniably influenced by temperature, making it a crucial aspect in the context of energy-driven mechanisms. The impact of temperature on the adsorption of fluoride ions was examined at four distinct temperatures: 298, 303, 308, and 313 K. It became apparent that as the temperature increased, the efficiency of adsorption decreased which is shown in Figure 9. This indicates the exothermic characteristic of the binding action of adsorption process. The observation had been made that adsorption progressively reduced when temperature increased, indicating an exothermic sorption mecha-

Table 3. Adsorption isotherm parameters for adsorption of fluoride on CSAC800

Isotherm model	Isotherm parameters	Temperature(K) 298K	Temperature(K) 303K	Temperature(K) 308K
Langmuir	Q_{max} (mg/g)	78.69	65.69	57.69
	K_L	3.29	3.29	3.29
	R^2	0.96	0.937	0.975
Freundlich	Q_{max} (mg/g)	60.058	52.23	43.94
	R^2	0.92	0.972	0.99
Temkin model	K_t	71.52	64.16	54.50
	R^2	0.96	0.93	0.97

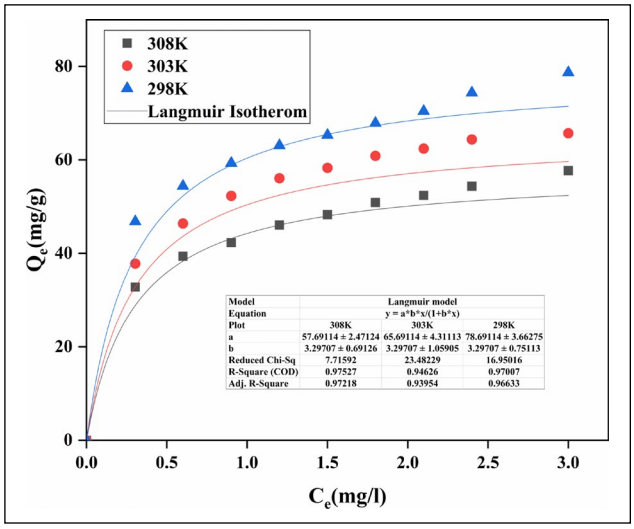

Figure 10. Langmuir isotherms describing the F^- adsorption; Solution pH 6.0±0.1, dose 0.5 g/L, contact time 24 h.

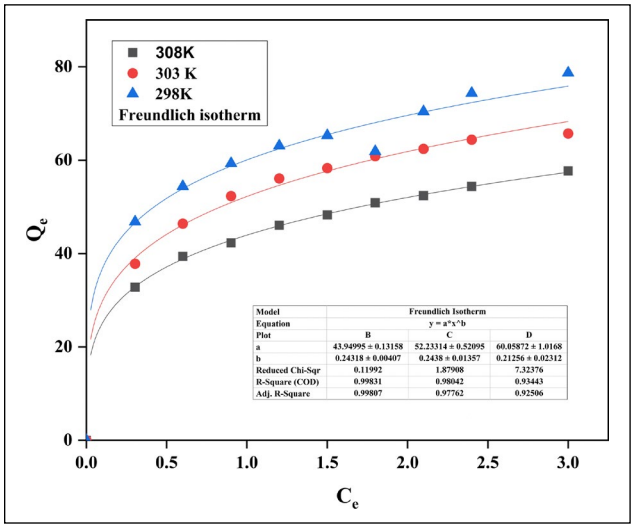

Figure 11. Freundlich isotherms describing the F^- adsorption; pH 6.0±0.1, dose 0.5 g/L, contact time 24 h.

nism. The reduced adsorption could have been the consequence of the adsorbate's greater propensity to move from the adsorbent exterior into contaminated sample, which would reduce the outer layer's thickness. Subsequently, there was a notable decline in fluoride decontamination efficiency by CSAC, because of substantial reductions in both the adsorption spots along with the fluoride level.

Adsorption Isotherms

For the purpose of examining the adsorption mechanism and delineating the relationship between the amount of F^- and the adsorbent's ability to hold on to CSAC, Several mathematical models are employed. The respective parameters are displayed in Table 3. The Langmuir model posits that a constant quantity of adsorption sites is accessible on the adsorbent's surface; every spot has the capacity to accommodate only a single molecule, in other words, this refers to monolayer adsorption, where the adsorption energy does not change throughout. The dual processes of monolayer and multilayer adsorption were explained by the Freundlich model. Additionally, it clarifies that the adsorbent possesses regions with different binding strengths signifying the existence of heterogeneous regions. Study using Temkin isotherms explains how adsorption energy gets distributed throughout the adsorbent's heterogeneous regions. At low adsorbate concentrations, the model exhibits behavior similar to the Langmuir isotherm and shifts to the Freundlich isotherm characteristics when the concentrations of adsorbate are high. Figure 10, 11 and 12 displays the non-linearized representations created from the data.

According to the relative characteristics, the Langmuir isotherm model adequately explains adsorption of F^-, which also makes clear that how the adsorption potential is distributed across the adsorbent's diverse regions. CSAC800 exhibited a maximal adsorption capacity of 78.69 mg/g, while at pH 6, the maximum capacity of 60.058 mg/g was observed in Freundlich isotherm. With a relatively excellent correlation value (R^2=0.975). In accordance with the R^2 value, the Langmuir isotherm offers the most suitable fit when compared to other isotherm models.

Moreover, K_L=3.29 L/mg was the mean figures corresponding to adsorption constant (saturation coefficient) in accordance with Langmuir equation. Alternatively, the Langmuir parameter (K_L) serves as an indicator of the level of bonding between the adsorbing material and the surface. A stronger contact within the adsorbent-adsorbate is indicated by a significantly increased value of K_L, while a lower figure suggests a weaker relationship.

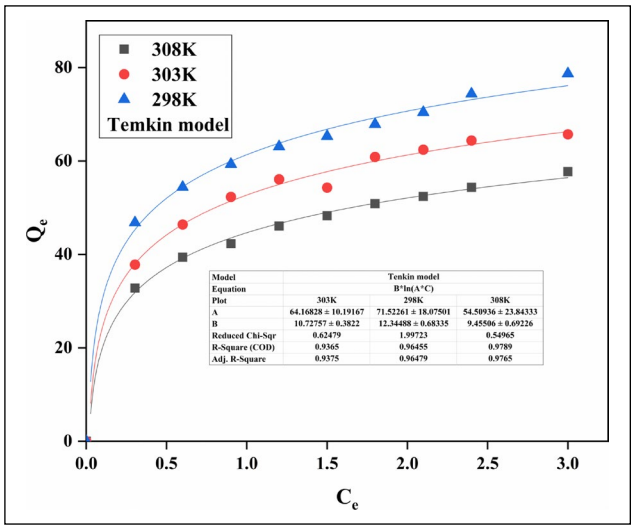

Figure 12. Temkin isotherms describing the F^- adsorption; pH 6.0±0.1, dose 0.5 g/L, contact time 24 h.

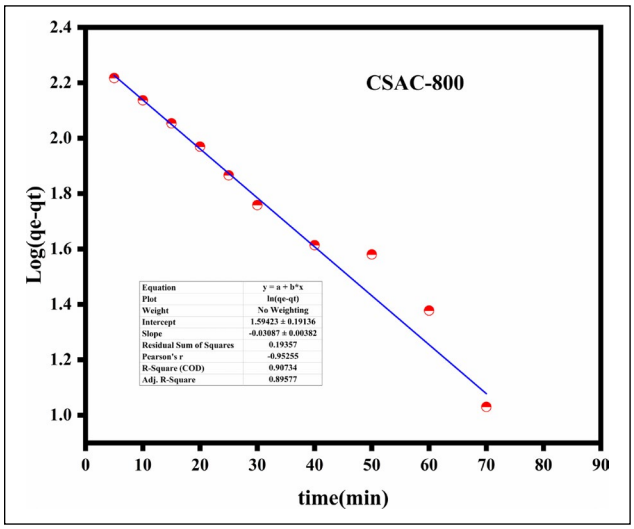

Figure 13. Kinetic PFO model for F^- adsorption; pH 6.0±0.1, dose 0.5 g/L, contact time 24 h.

In summary, the outcomes derived from employing the three-parameter equations indicated that the Langmuir represented the most appropriate fitted adsorption isotherm model and superior fit for standard equilibrium values compared with the two-parameter models.

Adsorption Kinetics and the Adsorption Mechanism for Fluoride Elimination

The adsorption kinetics of fluoride on CSAC800 were investigated under identical parameters at room temperature, specifically with a 0.5 g/L dosage of adsorbent, commencing concentration of F^- 10 mg/L, and pH 6.0±0.1. In the kinetic study, both the pseudo-first-order (PFO) and pseudo-second-order (PSO) models were employed to analyze the adsorption kinetics. The regression coefficients, rate constants (k), and equilibrium adsorption capacities (cal) for both the pseudo-first-order (PFO) and pseudo-second-order (PSO) kinetic models were determined by analyzing their corresponding linear graphs of log (q_e - q_t) against time (t) in Figure 13 and t/qt against time (t) in Figure 14.

By examining the resulting R^2 values of 0.902 for the PFO model and 0.997 for the PSO model, for CSAC800, at pH 6.0±0.1 as a reference point, it becomes evident that the PSO model fits well and is more appropriate. The coefficient of regression in the PSO context exceeds that of PFO, and the determined equilibrium adsorption capacity (q_e) derived from the linear depiction of PSO kinetics closely aligns with the empirical qe information. However, On the other hand, there seems to be a bit of a discrepancy in the q_e Figure 13 for PFO kinetics when comparing the observed value with the one deduced through computational means. The way F^- adsorbs on CSAC800 is better suited to PSO kinetics rather than PFO kinetics. This suggests that the process of adsorption is more efficient and effective when following the PSO model. However, a comparable outcome emerges when examining the non-linear representations of PFO and PSO kinetic models. In this case as well, the regression coefficient for PSO kinetics proves to be superior

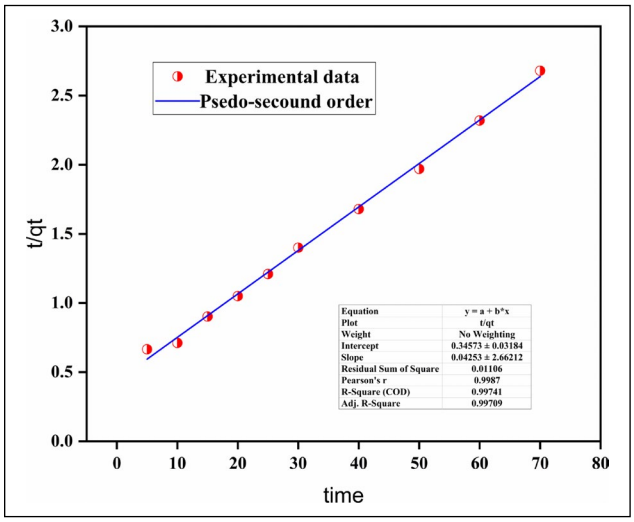

Figure 14. Kinetic PSO model for F^- adsorption; pH 6.0±0.1, dose 0.5 g/L, contact time 24 h.

to that of PFO kinetics. The computed parameters for the aforementioned models are detailed in Table 4. These findings demonstrated and validated that the chemical fluoride adsorption on CSAC800 was regulated because of electrostatic interactions followed by ion transfer [45].

Furthermore, it was evident that, the material's performance was at its maximal when the pH is set at 6. This pattern contradicts with the outcomes reported in earlier research that utilized modified adsorbents [50]. It was ascribed to the process of electrostatic interaction within the lower pH spectrum, which decreases as pH rises and results in a poor effectiveness around pH 6.

As previously determined, the process alters and ion exchange takes over at pH levels of 7 and higher. The process of fluoride removal via adsorption is intricate, encompassing diverse physical and chemical interactions between the fluoride ions and the adsorbent material. Understanding the mechanisms behind fluoride removal is crucial as it

Table 4. Kinetic parameters for PFO and PSO for adsorption of fluoride on CSAC800

Pseudo-first order	
q_e	4.92 (mg/g)
K_1	5.1×10^{-2} (g/mg min)
R^2	0.902
Pseudo-second order	
q_e	31.6 (mg/g)
K_2	4.2×10^{-2} (g/mg min)
R^2	0.997

aids in researching and enhancing the defluoridation capabilities of adsorbents. The mechanism for the elimination of fluoride by CSAC800 adsorbent is shown in Figure 15.

Thermodynamic Study

Utilizing thermodynamic analysis, the assessment of the capability and the spontaneous nature of the adsorption method was achieved by calculating three essential thermodynamic coefficients. These parameters include the free energy change (ΔG^0), entropy change (ΔS^0), and standard enthalpy change (ΔH^0). This is determined by utilizing and employing the following Van't Hoff formula:

$$K_0 = \frac{\Delta S^0}{R} - \frac{\Delta H^0}{RT} \quad (8)$$

$$K_0 = K_L \times 1000 \times molecular\ mass\ of\ adsorbing\ material \quad (9)$$

The gradient and intercept of the Van't Hoff graph, which illustrates $\ln K_0$ plotted against 1/T (Fig. 16), were employed for the determination of the thermodynamic parameters and the corresponding values are in Table 5. The reported values for ΔS^0 and ΔH^0 in removal of F^- ions are 19.59 kJ/mol/K and 8.57 kJ/mol respectively. These values imply a remarkably robust interaction and a decrease in the unpredictability of F^- ions after being adsorbed by CSAC800.

Table 5. Thermodynamic parameters for adsorption of fluoride on CSAC800

Temperature (K)	-ΔG kJ /mol	ΔH kJ /mol	ΔS kJ/ mol/K
298	2.41	8.7	19.59
303	1.441		
308	0.18		

In addition, negative reading of G^0 (ranging from 2.41 kJ/mol to 0.18 kJ/mol) at temperature fluctuation of 298K-308K indicates that overall adsorption appears both thermodynamically feasible and spontaneous. However, the diminishing negative figure of ΔG^0 at an increased temperature span indicates its decreasing spontaneity [68].

Regeneration Study/ Reusability

Regeneration studies were carried out to assess the reusability of CSAC800 in the removal of F^-. These experiments were conducted at a 7 pH, with 10 mg/L starting F^- level and 0.5 g/L as adsorbing material quantity. Following the completion of the first cycle, CSAC800 particulate matter were processed with a 0.01M NaOH solution and stirred for a period of 180 minutes, clean using deionized water imple-

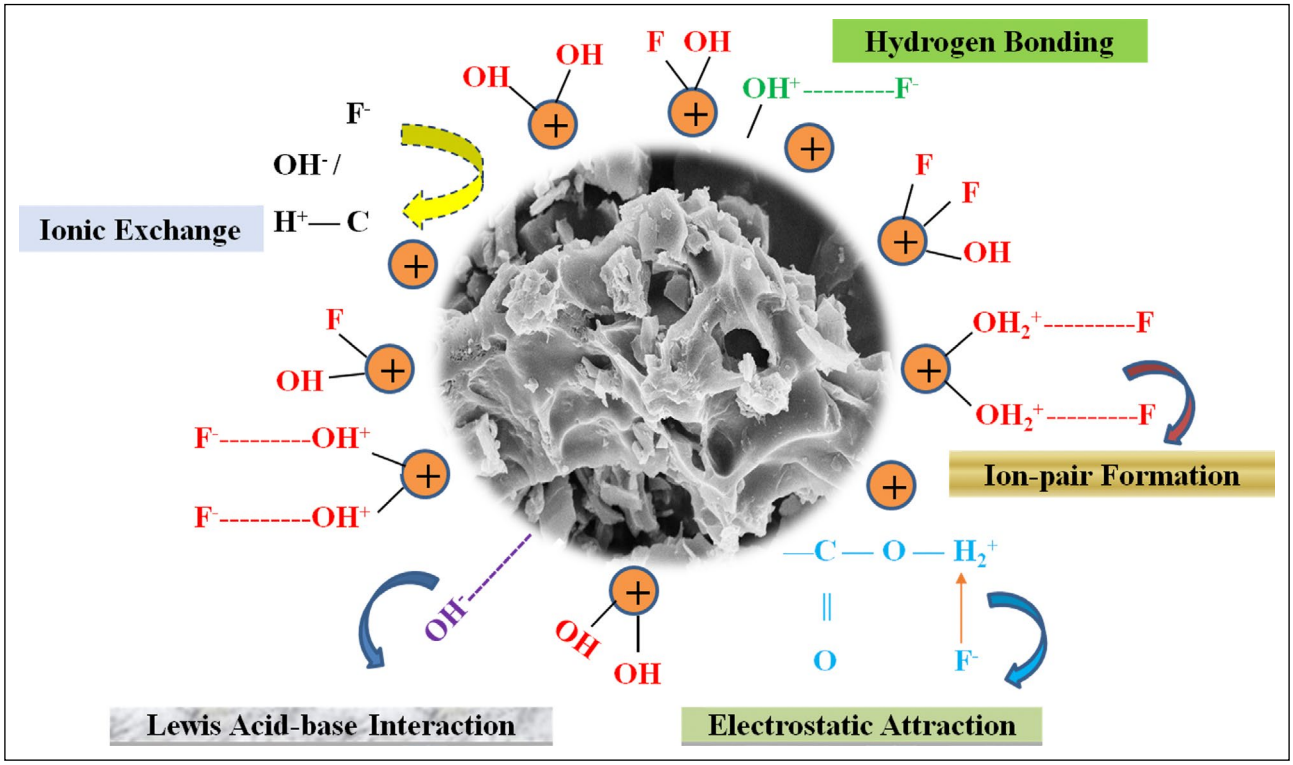

Figure 15. Mechanism of fluoride adsorption onto CSAC800.

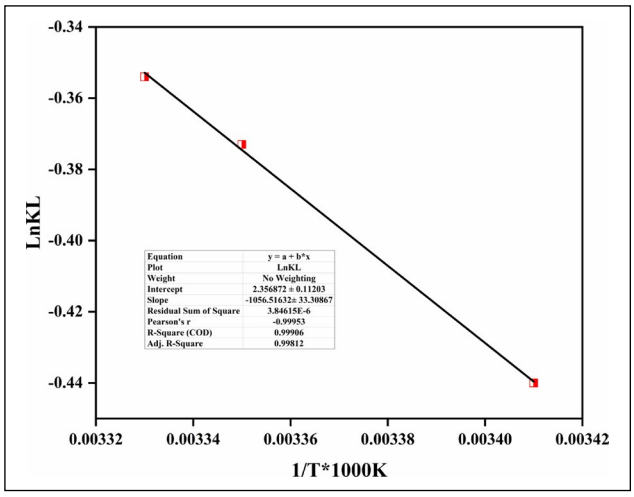

Figure 16. Plot showing the activation energy for the adsorption of F^- ions.

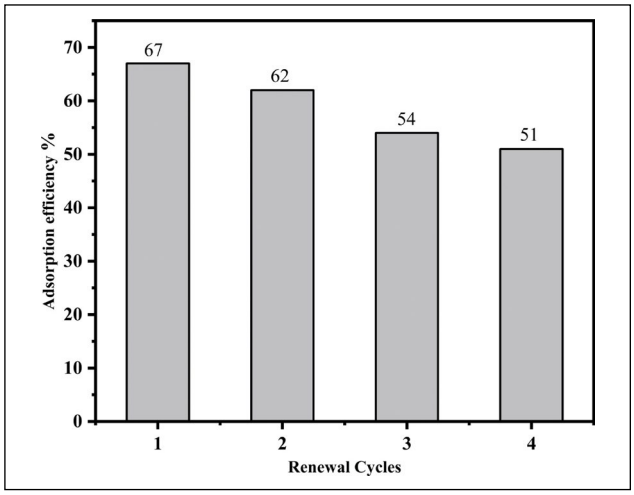

Figure 17. Fluoride adsorption on CSAC800 was investigated over four cycles after regeneration. Initial [F^-] was 10 mg/L, with pH 6.0±0.1, 0.5 g/L dose, 25±1°C temperature, and 5-hour contact time.

mented sequentially to eliminate any surplus base quantity. Appropriate repetition interval was chosen for each cycle. As depicted in Figure 17, the adsorbent, following desorption, was subjected to testing for four consecutive cycles for F^- removal. During the initial 1st cycle, the F^- removal percentage stood at approximately 68%, and by the conclusion of the 4th cycle, it had reduced to around 51%. Consequently, this study provided evidence of the CSAC800 adsorbent's ability to be employed for F^- removal across four repeated cycles, after being effectively restored with NaOH processing. Upon 4 renewal stages, the F^- elimination capability has solely dropped by 10%.

CONCLUSION

Chestnut shell-derived activated carbon was employed for the elimination of fluoride ions from water-based solutions. The efficacy of different composite materials (CSC800, CSCAC600, CSAC700 and CSAC800) was evaluated under different conditions, and the resulting order of effectiveness was as follows: CSAC800> SCAC700> SCAC600> CSC800. The prepared materials underwent characterization through the utilization of scanning electron microscopy (SEM), Fourier-transform infrared spectroscopy (FTIR), and Brunauer-Emmett-Teller (BET) techniques. CSAC800 exhibited a measured BET surface area of 912.38 m^2/g and a pore volume of 0.188 cm^3/g. SEM analysis indicated that the material possessed a porous and uniform structure, with the CSAC800 sample exhibiting a higher number of cavities. Among the carbon samples CSAC800, displayed the fewest cavities, but it had a larger pore size. Furthermore, FTIR analysis corroborated the presence of multiple bonds, among other chemical bonds. The performance evaluation of the CSAC800 material revealed that a dosage of 0.5 g/L was sufficient to reduce the fluoride concentration to less than 2.5 mg/L. The maximal adsorption capability for CSAC800 was determined to be 78.69 mg/g, while for CSAC700, it was found to be 26 mg/g. In batch experiments, a contact time of 5 hours (300 minutes) was identified as the optimal duration. Additionally, the pseudo second order model provided a better fit for CSAC800 materials in describing the adsorption kinetics. The adsorbent's reusability was evaluated through consecutive adsorption and regeneration studies, employing 0.01 M NaOH as the eluent. The findings indicated that even after four (4) regeneration cycles, the adsorption capacity only experienced a marginal decline of 10%, demonstrating the adsorbent's favorable potential for multiple uses. The elimination of fluoride through adsorption is an intricate procedure, entailing numerous physical and chemical interactions between the fluoride ions and the adsorbent material.

ACKNOWLEDGEMENTS

The authors thankfully acknowledge the National Institute of Technology Srinagar, Jammu and Kashmir, India.

DATA AVAILABILITY STATEMENT

The author confirm that the data that supports the findings of this study are available within the article. Raw data that support the finding of this study are available from the corresponding author, upon reasonable request.

CONFLICT OF INTEREST

The author declared no potential conflicts of interest with respect to the research, authorship, and/or publication of this article.

USE OF AI FOR WRITING ASSISTANCE

Not declared.

ETHICS

There are no ethical issues with the publication of this manuscript.

REFERENCES

[1] S. Arya, T. Subramani, G. Vennila, and D. Karunanidhi, "Health risks associated with fluoride intake from rural drinking water supply and inverse mass balance modeling to decipher hydrogeochemical processes in Vattamalaikarai River basin, South India," Environmental Geochemistry and Health, Vol. 43, pp. 705–716, 2021. [CrossRef]

[2] S. Ahmadi, M. Mesbah, C.A. Igwegbe, C.D. Ezeliora, C. Osagie, N.A. Khan, G.L. Dotto, M. Salari, and M.H. Dehghani, Sono electro-chemical synthesis of LaFeO3nanoparticles for the removal of fluoride: Optimization and modeling using RSM, ANN and GA tools, Journal of Environmental Chemical Engineering, Vol. 9, Article 105320, 2021. [CrossRef]

[3] R.W. Premathilaka, and N.D. Liyanagedera, "Fluoride in drinking water and nanotechnological approaches for eliminating excess fluoride," Journal of Nanotechnology, Vol. 2019, Article 2192383, 2019. [CrossRef]

[4] F. A. Dar, and S. Kurella, "Recent advances in adsorption techniques for fluoride removal – An overview," Groundwater for Sustainable Development, Vol. 23, Article 101017, 2023. [CrossRef]

[5] F. Ahmad Dar, S. Kurella, Fluoride in drinking water: An in-depth analysis of its prevalence, health effects, advances in detection and treatment, Materials Today: Proceedings, 2023. [Epub ahead of print]. doi: 10.1016/j.matpr.2023.05.645. [CrossRef]

[6] G. Jacks, P. Bhattacharya, V. Chaudhary, and K. P. Singh, "Controls on the genesis of some high-fluoride groundwaters in India," Applied Geochemistry, Vol. 20, pp. 221–228, 2005. [CrossRef]

[7] A.I. Ndé-Tchoupé, R. Tepong-Tsindé, M. Lufingo, Z. Pembe-Ali, I. Lugodisha, R.I. Mureth, M. Nkinda, J. Marwa, W. Gwenzi, T.B. Mwamila, M.A. Rahman, C. Noubactep, and K.N. Njau, "White teeth and healthy skeletons for all: The path to universal fluoride-free drinking water in Tanzania," Water (Switzerland), Vol. 11, 2019. [CrossRef]

[8] K.K. Yadav, S. Kumar, Q.B. Pham, N. Gupta, S. Rezania, H. Kamyab, S. Yadav, J. Vymazal, V. Kumar, D.Q. Tri, A. Talaiekhozani, S. Prasad, L.M. Reece, N. Singh, P.K. Maurya, and J. Cho, "Fluoride contamination, health problems and remediation methods in Asian groundwater: A comprehensive review," Ecotoxicology and Environmental Safety, Vol. 182, Article 109362, 2019. [CrossRef]

[9] S. Ali, S. Shekhar, P. Bhattacharya, G. Verma, T. Chandrasekhar, and A. K. Chandrashekhar, "Elevated fluoride in groundwater of Siwani Block, Western Haryana, India: A potential concern for sustainable water supplies for drinking and irrigation," Groundwater for Sustainable Development, Vol. 7, pp. 410–420, 2018. [CrossRef]

[10] M. Vithanage, P. Bhattacharya, Fluoride in the environment: sources, distribution and defluoridation, Environmental Chemistry Letters. Vol. 13, pp. 131–147, 2015. [CrossRef]

[11] M. Vithanage, P. Bhattacharya, Fluoride in Drinking Water: Health Effects and Remediation, in: S. E., R. J. (Eds.), Lichtfouse, Springer, Environmental Chemistry for a Sustainable World: Volume 5: CO2 Sequestration, Biofuels and Depollution. International Publishing, Switzerland, pp. 105–151, 2015. [CrossRef]

[12] J. Ijumulana, F. Ligate, R. Irunde, P. Bhattacharya, J.P. Maity, A. Ahmad, and F. Mtalo, "Spatial uncertainties in fluoride levels and health risks in endemic fluorotic regions of northern Tanzania," Groundwater for Sustainable Development, Vol. 14, Article 100618, 2021. [CrossRef]

[13] V. Kimambo, P. Bhattacharya, F. Mtalo, J. Mtamba, A. Ahmad, Fluoride occurrence in groundwater systems at global scale and status of defluoridation – State of the art, Groundwater for Sustainable Development, Vol. 9, Article 100223, 2019. [CrossRef]

[14] R.W. Herschy, Water quality for drinking: WHO guidelines, "Encyclopedia of Earth Sciences Series," pp. 876–883, 2012. [CrossRef]

[15] A. K. Tolkou, N. Manousi, G.A. Zachariadis, I.A. Katsoyiannis, and E. A. Deliyanni, Recently developed adsorbing materials for fluoride removal from water and fluoride analytical determination techniques: A review," Sustainability (Switzerland), Vol. 13, Article 7061, 2021. [CrossRef]

[16] A. Mohamed, E. P. Valadez Sanchez, E. Bogdanova, B. Bergfeldt, A. Mahmood, R. V. Ostvald, and T. Hashem, "Efficient fluoride removal from aqueous solution using zirconium-based composite nanofiber membranes," Membranes, Vol. 11, pp. 1–13, 2021. [CrossRef]

[17] M. Grzegorzek, K. Majewska-Nowak, and A. E. Ahmed, "Removal of fluoride from multicomponent water solutions with the use of monovalent selective ion-exchange membranes," Science of the Total Environment, Vol. 722, 2020. [CrossRef]

[18] A. K. Tolkou, M. Mitrakas, I. A. Katsoyiannis, M. Ernst, and A. I. Zouboulis, "Fluoride removal from water by composite Al/Fe/Si/Mg pre-polymerized coagulants: Characterization and application," Chemosphere, Vol. 231, pp. 528–537, 2019. [CrossRef]

[19] Y. Wang, and E. J. Reardon, "Activation and regeneration of a soil sorbent for defluoridation of drinking water," Applied Geochemistry, Vol. 16, pp. 531–539, 2001. [CrossRef]

[20] Y. Gan, X. Wang, L. Zhang, B. Wu, G. Zhang, S. Zhang, Coagulation removal of fluoride by zirconium tetrachloride: Performance evaluation and mechanism analysis, Chemosphere, Vol. 218, pp. 860–868, 2019. [CrossRef]

[21] K.K. Yadav, N. Gupta, V. Kumar, S.A. Khan, and A. Kumar, "A review of emerging adsorbents and current demand for defluoridation of water: Bright future in water sustainability," Environment International, Vol. 111 pp. 80–108, 2018. [CrossRef]

[22] P. S. Kumar, S. Suganya, S. Srinivas, S. Priyadharshini, M. Karthika, R. Karishma Sri, V. Swetha, M. Naushad, and E. Lichtfouse, "Treatment of fluoride-contaminated water. A review," Environmental Chemistry Letters, Vol. 17, pp. 1707–1726, 2019. [CrossRef]

[23] R. Kumar, S. Ali, S. Sandanayake, M.A. Islam, J. Ijumulana, J.P. Maity, M. Vithanage, M.A. Armienta, P. Sharma, R. Hamisi, V. Kimambo, and P. Bhattacharya, "Fluoride as a global groundwater contaminant," in: R. Naidu (Ed.), Inorganic Contaminants and Radionuclides, Elsevier, pp. 319–350, 2023. [CrossRef]

[24] B. Van der Bruggen, M. Mänttäri, and M. Nyström, "Drawbacks of applying nanofiltration and how to avoid them: A review," Separation and Purification Technology, Vol. 63, pp. 251–263, 2008. [CrossRef]

[25] Y. Du, D. Wang, W. Wang, J. Fu, X. Chen, L. Wang, W. Yang, and X. Zhang, "Electrospun Nanofibrous Polyphenylene Oxide Membranes for High-Salinity Water Desalination by Direct Contact Membrane Distillation," ACS Sustainable Chemistry and Engineering," Vol. 7, pp. 20060–20069, 2019. [CrossRef]

[26] S. Jagtap, M.K. Yenkie, N. Labhsetwar, and S. Rayalu, "Fluoride in drinking water and defluoridation of water," Chemical Reviews, Vol. 112, pp. 2454–2466, 2012. [CrossRef]

[27] M. Sadhu, P. Bhattacharya, M. Vithanage, and P. Padmaja Sudhakar, "Adsorptive removal of fluoride using biochar – A potential application in drinking water treatment," Separation and Purification Technology, Vol. 278, Article 119106, 2021. [CrossRef]

[28] M. M. Mahmoudi, S. Nasseri, A. H. Mahvi, A. Dargahi, M. S. Khubestani, and M. Salari, "Fluoride removal from aqueous solution by acid-treated clinoptilolite: Isotherm and kinetic study," Desalination and Water Treatment, Vol. 146, pp. 333–340, 2019. [CrossRef]

[29] R. Kumar, P. Sharma, W. Yang, M. Sillanpää, J. Shang, P. Bhattacharya, M. Vithanage, and J. P. Maity, "State-of-the-art of research progress on adsorptive removal of fluoride-contaminated water using biochar-based materials: Practical feasibility through reusability and column transport studies," Environmental Research, Vol. 214, Article 114043, 2022. [CrossRef]

[30] M. T. Samadi, M. Zarrabi, M.N. Sepehr, S. M. Ramhormozi, S. Azizian, and A. Amrane, "Removal of fluoride ions by ion exchange resin: Kinetic and equilibrium studies," Environmental Engineering and Management Journal, Vol. 13, pp. 205–214, 2014. [CrossRef]

[31] T. Pang, T. S. Aye Chan, Y.A.C. Jande, and J. Shen, "Removal of fluoride from water using activated carbon fibres modified with zirconium by a drop-coating method," Chemosphere, Vol. 255, Article 126950, 2020. [CrossRef]

[32] R. Kumar, P. Sharma, P.K. Rose, P.K. Sahoo, P. Bhattacharya, A. Pandey, and M. Kumar, "Co-transport and deposition of fluoride using rice husk-derived biochar in saturated porous media: Effect of solution chemistry and surface properties," Environmental Technology and Innovation, Vol. 30, Article 103056, 2023. [CrossRef]

[33] M. Tazik, M.H. Dehghani, K. Yaghmaeian, S. Nazmara, M. Salari, A.H. Mahvi, S. Nasseri, H. Soleimani, and R.R. Karri, "4-Chlorophenol adsorption from water solutions by activated carbon functionalized with amine groups: response surface method and artificial neural networks," Scientific Reports, Vol. 13, pp. 1–20, 2023. [CrossRef]

[34] H.M. Duong, T.Q. Tran, R. Kopp, S.M. Myint, and L. Peng, "Direct spinning of horizontally aligned carbon nanotube fibers and films from the floating catalyst method," Elsevier, Inc, 2019.

[35] H. M. Duong, S. M. Myint, T. Q. Tran, and D. K. Le, "Post-spinning treatments to carbon nanotube fibers," Elsevier, Ltd, 2019. [CrossRef]

[36] L. Delgadillo-Velasco, V. Hernández-Montoya, F.J. Cervantes, M. A. Montes-Morán, and D. Lira-Berlanga, "Bone char with antibacterial properties for fluoride removal: Preparation, characterization and water treatment," Journal of Environmental Management, Vol. 201, pp. 277–285, 2017.

[37] J. Chen, R. Yang, Z. Zhang, and D. Wu, "Removal of fluoride from water using aluminum hydroxide-loaded zeolite synthesized from coal fly ash," Journal of Hazardous Materials, Vol. 421, Article 126817, 2022. [CrossRef]

[38] N. Nabbou, M. Belhachemi, M. Boumelik, T. Merzougui, D. Lahcene, Y. Harek, A.A. Zorpas, and M. Jeguirim, "Removal of fluoride from groundwater using natural clay (kaolinite): Optimization of adsorption conditions," Comptes Rendus Chimie, Vol. 22, pp. 105–112, 2019. [CrossRef]

[39] G.Z. Kyzas, A.K. Tolkou, T.J. Al Musawi, N. Mengelizadeh, S. Mohebi, and D. Balarak, "Fluoride removal from water by using green magnetic activated carbon derived from canola stalks," Water, Air, and Soil Pollution, Vol. 233, 2022. [CrossRef]

[40] E. Vences-Alvarez, J. L. Flores-Arciniega, H. Flores-Zuñiga, and J. R. Rangel-Mendez, "Fluoride removal from water by ceramic oxides from cerium and manganese solutions," Journal of Molecular Liquids, Vol. 286, Article 11088, 2019. [CrossRef]

[41] A. K. Chaturvedi, K. C. Pathak, and V. N. Singh, "Fluoride removal from water by adsorption on china clay," Applied Clay Science, Vol. 3, pp. 337–346, 1988. [CrossRef]

[42] P. Pillai, S. Dharaskar, M. Shah, and R. Sultania, "Determination of fluoride removal using silica nano adsorbent modified by rice husk from water," Groundwater for Sustainable Development, Vol. 11, Article 10042, 2020. [CrossRef]

[43] R. R. Devi, I. M. Umlong, P. K. Raul, B. Das, S. Banerjee, and L. "Singh, Defluoridation of water using nano-magnesium oxide," Journal of Experimental Nanoscience, Vol. 9, pp. 512–524, 2014. [CrossRef]

[44] J. Zhou, W. Zhu, J. Yu, H. Zhang, Y. Zhang, X. Lin, and X. Luo, "Highly selective and efficient removal of fluoride from ground water by layered Al-Zr-La Tri-metal hydroxide," Applied Surface Science, Vol. 435, pp. 920–927, 2018. [CrossRef]

[45] N. Zhou, X. Guo, C. Ye, L. Yan, W. Gu, X. Wu, Q. Zhou, Y. Yang, X. Wang, and Q. Cheng, "Enhanced fluoride removal from drinking water in wide pH range using La/Fe/Al oxides loaded rice straw biochar," Water Supply, Vol. 22, pp. 779–794, 2022. [CrossRef]

[46] A. Amalraj, and A. Pius, "Removal of fluoride from drinking water using aluminum hydroxide coated activated carbon prepared from bark of Morinda tinctoria," Applied Water Science, Vol. 7, pp. 2653–2665, 2017. [CrossRef]

[47] C. E. Choong, K.T. Wong, S. B. Jang, I. W. Nah, J. Choi, S. Ibrahim, Y. Yoon, and M. Jang, "Fluoride removal by palm shell waste based powdered activated carbon vs. functionalized carbon with magnesium silicate: Implications for their application in water treatment," Chemosphere, Vol. 239, Article 124765, 2020. [CrossRef]

[48] N. Minju, K. Venkat Swaroop, K. Haribabu, V. Sivasubramanian, and P. Senthil Kumar, "Removal of fluoride from aqueous media by magnesium oxide-coated nanoparticles," Desalination and Water Treatment, Vol. 53, pp. 2905–2914, 2015. [CrossRef]

[49] P. Wu, L. Xia, Y. Liu, J. Wu, Q. Chen, and S. Song, "Simultaneous sorption of arsenate and fluoride on calcined Mg-Fe-La hydrotalcite-like compound from water," ACS Sustainable Chemistry and Engineering, Vol. 6, pp. 16287–16297, 2018. [CrossRef]

[50] A. K. Tolkou, S. Trikalioti, O. Makrogianni, D. G. Trikkaliotis, E. A. Deliyanni, G. Z. Kyzas, and I. A. Katsoyiannis, "Magnesium modified activated carbons derived from coconut shells for the removal of fluoride from water," Sustainable Chemistry and Pharmacy, Vol. 31, Article 100898, 2023. [CrossRef]

[51] L. X. Li, D. Xu, X. Q. Li, W. C. Liu, and Y. Jia, "Excellent fluoride removal properties of porous hollow MgO microspheres," New Journal of Chemistry, Vol. 38, pp. 5445–5452, 2014. [CrossRef]

[52] C. Sairam Sundaram, N. Viswanathan, S. Meenakshi, Defluoridation of water using magnesia/chitosan composite, Journal of Hazardous Materials, Vol. 163, pp. 618–624, 2009. [CrossRef]

[53] S. A. Mousavi, B. Kamarehie, A. Almasi, M. Darvishmotevalli, M. Salari, M. Moradnia, F. Azimi, M. Ghaderpoori, Z. Neyazi, and M. A. Karami, "Removal of Rhodamine B from aqueous solution by stalk corn activated carbon: adsorption and kinetic study," Biomass Conversion and Biorefinery, Vol. 13, pp. 7927–7936, 2023. [CrossRef]

[54] A. Alahabadi, N. Shomoossi, F. Riahimanesh, and M. Salari, "Development of AC/ZnO/Fe2O3 for efficiently adsorptive removal of Tetracycline from water environment: isotherm, kinetic and thermodynamic studies and adsorption mechanism," Biomass Conversion and Biorefinery, Vol. 14, pp. 17499–17517, 2023. [CrossRef]

[55] B. Devi, N.P. Baruah, A. Bharadwaj, and A. Devi, "Adsorptive removal of fluoride ions from aqueous solution using activated carbon supported tetrametallic oxide system," Chemical Engineering Research and Design, Vol. 197, pp. 380–391, 2023. [CrossRef]

[56] D. Cheng, H.H. Ngo, W. Guo, S.W. Chang, D.D. Nguyen, X. Zhang, S. Varjani, and Y. Liu, "Feasibility study on a new pomelo peel derived biochar for tet-racycline antibiotics removal in swine wastewater," Science of the Total Environment, Vol. 720 Article 137662, 2020. [CrossRef]

[57] H. Zhou, X. Li, H. Jin, and D. She, "Mechanism of a double-channel nitrogen-doped lignin-based carbon on the highly selective removal of tetracycline from water," Bioresource Technology, Vol. 346, Article 126652, 2022. [CrossRef]

[58] M. Wei, F. Marrakchi, C. Yuan, X. Cheng, D. Jiang, F.F. Zafar, Y. Fu, S. Wang, Adsorption modeling, thermodynamics, and DFT simulation of tetracycline onto mesoporous and high-surface-area NaOH-activated macroalgae carbon, Journal of Hazardous Materials, Vol. 425, Article 12788, 2022. [CrossRef]

[59] J. Qu, X. Lin, Z. Liu, Y. Liu, Z. Wang, S. Liu, Q. Meng, Y. Tao, Q. Hu, and Y. Zhang, "One-pot synthesis of Ca-based magnetic hydrochar derived from consecutive hydrothermal and pyrolysis processing of bamboo for high-performance scavenging of Pb(II) and tetracycline from water," Bioresource Technology, Vol. 343 Article 126046, 2022. [CrossRef]

[60] H. Zhang, X. Song, J. Zhang, Y. Liu, H. Zhao, J. Hu, and J. Zhao, "Performance and mechanism of sycamore flock based biochar in removing oxytetracycline hydrochloride," Bioresource Technology, Vol. 350 Article 126884, 2022. [CrossRef]

[61] J. E. Kim, S. K. Bhatia, H. J. Song, E. Yoo, H. J. Jeon, J. Y. Yoon, Y. Yang, R. Gurav, Y. H. Yang, H. J. Kim, and Y. K. Choi, "Adsorptive removal of tetracycline from aqueous solution by maple leaf-derived biochar," Bioresource Technology, Vol. 306, Article 123092, 2020. [CrossRef]

[62] W. Bae, J. Kim, and J. Chung, "Production of granular activated carbon from food-processing wastes (walnut shells and jujube seeds) and its adsorptive properties," Journal of the Air and Waste Management Association, Vol. 64, pp. 879–886, 2014. [CrossRef]

[63] S. Cheng, L. Zhang, H. Xia, J. Peng, S. Zhang, and S. Wang, "Preparation of high specific surface area activated carbon from walnut shells by microwave-induced KOH activation," Journal of Porous Materials, Vol. 22, pp. 1527–1537, 2015. [CrossRef]

[64] B. Li, Y. Zhang, J. Xu, Y. Mei, S. Fan, and H. Xu, "Effect of carbonization methods on the properties of tea waste biochars and their application in tetra-cycline removal from aqueous solutions," Chemo-sphere, Vol. 267, Article 129283, 2021. [CrossRef]

[65] K. Zhu, Y. Duan, F. Wang, P. Gao, H. Jia, C. Ma, and C. Wang, "Silane-modified halloysite/Fe3O4nano-composites: Simultaneous removal of Cr(VI) and Sb(V) and positive effects of Cr(VI) on Sb(V) adsorption," Chemical Engineering Journal, Vol. 311, pp. 236–246, 2017. [CrossRef]

[66] M. Zhang, L. Xu, C. Qi, and M. Zhang, "Highly effective removal of tetracycline from water by hierarchical porous carbon: Batch and column adsorption," Industrial and Engineering Chemistry Research, Vol. 58, pp. 20036–20046, 2019. [CrossRef]

[67] J. Zhang, M. Lu, J. Wan, Y. Sun, H. Lan, and X. Deng, "Effects of pH, dissolved humic acid and Cu2+ on the adsorption of norfloxacin on montmorillonite-biochar composite derived from wheat straw," Biochemical Engineering Journal, Vol. 130, 104–112, 2018. [CrossRef]

[68] S. Kalita, M. Pathak, G. Devi, H.P. Sarma, K.G. Bhattacharyya, A. Sarma, and A. Devi, "Utilization of: Euryale ferox Salisbury seed shell for removal of basic fuchsin dye from water: Equilibrium and kinetics investigation," RSC Advances, Vol. 7, pp. 27248–27259, 2017. [CrossRef]

[69] L. Huang, Z. Yang, Z. Zhang, L. Jin, W. Yang, Y. He, L. Ren, and H. Wang, "Enhanced surface hydroxyl groups by using hydrogen peroxide on hollow tubular alumina for removing fluoride," Microporous and Mesoporous Materials, Vol. 297, Article 110051, 2020. [CrossRef]

[70] P. Dhanasekaran, O. Sahu, Arsenate and fluoride removal from groundwater by sawdust impregnated ferric hydroxide and activated alumina (SFAA), Groundwater for Sustainable Development. Vol. 12, Article 100490, 2021. [CrossRef]

[71] M. Mouelhi, S. Giraudet, A. Amrane, B. Hamrouni, Competitive adsorption of fluoride and natural organic matter onto activated alumina, Environmental Technology (United Kingdom)," Vol. 37, pp. 2326–2336, 2016. [CrossRef]

[72] S. Wu, K. Zhang, J. He, X. Cai, K. Chen, Y. Li, B. Sun, L. Kong, and J. Liu, "High efficient removal of fluoride from aqueous solution by a novel hydroxyl aluminum oxalate adsorbent," Journal of Colloid and Interface Science, Vol. 464, pp. 238–245, 2016. [CrossRef]

[73] S.K. Swain, T. Patnaik, V.K. Singh, U. Jha, R.K. Patel, and R. K. Dey, "Kinetics, equilibrium and thermodynamic aspects of removal of fluoride from drinking water using meso-structured zirconium phosphate," Chemical Engineering Journal, Vol. 171, pp. 1218–1226, 2011. [CrossRef]

[74] J. Wang, N. Chen, C. Feng, and M. Li, "Performance and mechanism of fluoride adsorption from groundwater by lanthanum-modified pomelo peel biochar," Environmental Science and Pollution Research, Vol. 25, pp. 15326–15335, 2018. [CrossRef]

[75] W. Kim, R. Singh, and J. A. Smith, "Modified crushed oyster shells for fluoride removal from water," Scientific Reports, Vol. 10, pp. 1–13, 2020. [CrossRef]

[76] J. I. Lee, J. K. Kang, S. H. Hong, C. G. Lee, S. Jeong, and S. J. Park, "Thermally treated Mytilus coruscus shells for fluoride removal and their adsorption mechanism," Chemosphere, Vol. 263, Article 128328, 2021. [CrossRef]